Available online at www.eccomasproceedia.org
Eccomas Proceedia COMPDYN (2023) 3105-3121

ECCOMAS
Proceedia

COMPDYN 2023
9th ECCOMAS Thematic Conference on
Computational Methods in Structural Dynamics and Earthquake Engineering
M. Papadrakakis, M. Fragiadakis (eds.)
Athens, Greece, 12-14 June 2023

EQUIVALENT DAMPING RATIO EVALUATION FOR HISTORICAL CHURCH REINFORCED BY CROSS LAM ROOF STRUCTURE FOR IMPROVING THE SEISMIC RESPONSE

N. Longarini[1] **, P. Crespi**[1], **M. Zucca**[2]

[1] Department of Architecture, Built Environment and Construction Engineering Politecnico di Milano
Piazza Leonardo da Vinci 32, Milano, Italy
{nicola.longarini,pietro.crespi }@polimi.it

[2]Department of Civil, Environmental Engineering and Architecture University of Cagliari, Italy
Via Marengo, 2, Cagliari, Italy
e-mail: marco.zucca2@unica.it

Abstract

The paper is focused on the evaluation of the Equivalent Damping Ratio (EDR) obtained by different cross lam roof structures for an historical church for improving the seismic response. The church has one nave configuration, masonry walls and original wooden roof-structures. The seismic response of this kind of construction is afflicted by the nave transversal response, therefore structural improvements inspired to the global box behavior must be pursued for avoiding the out-of-plane mechanisms of the perimetral walls. The dissipative roof-diaphragm able to contain the lateral displacements and to permit a controlled rocking is studied by choosing pithed panel cross lam timber (CLT) panels. The wooden based solutions permit to use materials compatible to the original ones as requested by Cultural Heritage Office. By this way the dissipative effect due to the CLT roof structure must be calibrated by a careful choice of the steel connections, in terms of stiffness and strength. The optimization of connections dissipative effects is here carried out by the estimation of EDR with three methods: FEMA 440, ATC-40 and time histories (TH). Each method is applied to equivalent finite elements models in which the nonlinear properties of the masonry walls and wooden roof with steel connections are considered by inelastic rotational springs (for the walls) and inelastic shear springs (for the roof). A comparison of the EDR values is shown and discussed.

Keywords: Historical buildings, Cross Lam Timber Structure; Effective Equivalent Damping; Seismic Vulnerability, Nave Transversal Response

ISSN:2623-3347
Peer-review under responsibility of the organizing committee of COMPDYN 2023.
doi: 10.7712/120123.10626.20123

1 INTRODUCTION

The paper is focused on the seismic response optimization of historical one-nave configuration churches with masonry structures and wooden roof by the estimation of the Equivalent Damping Ratio (EDR) indicated by symbol β_{eq} in FEMA 440 [1] or the definition Effective Viscous Damping and symbol β_{eff} in ATC-40 [2].

In the post-earthquake survey, under transversal earthquake this kind of construction has shown several recurring collapse mechanisms as out-of-plane mechanisms of the perimeter walls or excessive in-plane stresses afflicting the seismic resistance elements [3],[4].

To avoid these mechanisms, a dissipative roof diaphragm represents a valid technique especially when it is not adequate to use steel chains for the poor quality of the masonry or for excessive geometrical slenderness of the perimeter walls.

The roof diaphragm can be represented by wooden elements and steel connections also considering the preservation of the original materials of the historical churches. The wooden pitched panels replacing or over-layering the original wooden planks must withstand to the in-plane shear stresses and the steel connections must be calibrated in terms of strength and stiffness to resist and to dissipate the inertia forces due to the seismic action. For these reasons Cross Lam Timber (CLT) panels can be used representing a valid precast solution with in-plane higher resistance with respect to the original wooden planks[5]. Moreover, the generic CLT panel is a smart technology thanks to its coupled hardwood layers, having 90° orientation themselves, able to reduce the resistance problems of the single planks related to the single orientation of the grains regardless of the total thickness.

With the CLT panels technology, the energy's dissipation must be occurred in the steel connections. In case nave transversal response in one nave configuration church, the panel-to-panel connections play a crucial role in the energy's dissipation either for reducing the in-plane shear actions stressing the wooden elements of the roof and for reducing the forces transmitted by the roof to the façade. The calibration of the stiffness due to the connections permits to control the lateral displacements of the church but it is mandatory to not create an over stiffness solution because the façade could be afflicted by in-plane shear stresses not compatible to the mechanical features of the masonry elements.

In the present paper the energy dissipation under transversal seismic action obtained by CLT panels with steel connections (in different geometrical configurations) is given in terms of EDR evaluated for the global construction[6], considering the contributes of the masonry walls and wooden roof diaphragm. The optimization of EDR is shown in relation to the transversal displacements obtained with different geometrical configuration of the steel connections. Therefore, a case study church is represented by equivalent finite element model (FEM) with nonlinear proprieties for the equivalent vertical elements – representing the head and perimeter walls) – and the equivalent horizontal elements – representing the wooden panels with the steel connections -. In the FEM, nonlinear properties can be introduced by inelastic hinges: (i) inelastic rotational hinges located at the base of the vertical elements represent the inelastic behavior of the masonry perimeter walls involved in the nave transversal response whereas (ii) shear inelastic hinges to attribute to the horizonal elements describe the dissipation occurring in the roof's in-plane connections[7,8]. The nonlinear behavior of the inelastic hinges represents an important issue in the performance based seismic design for several reasons. If the nonlinear behavior of the rotation hinges is evaluated by the geometrical and mechanical features of the existent masonry walls, the inelastic properties of the shear inelastic hinges of the roof can be opportunely changed to obtain the best result in terms of EDR. By adopting equivalent FEM, the EDR estimation can be performed without a strong computational effort by varying the properties of the shear inelastic hinges in relation to the geometrical features of

the CLT roof-diaphragm in terms of thickness of the panels and steel connections configuration (diameter of the connections, mutual distance and stiffness of the single connection evaluated by [9] as K_{ser}).

In this paper, the EDR is estimated by performing nonlinear static (pushover) and nonlinear dynamic analyses (time histories) where the inelastic features of the walls and the roof are introduced by the above-mentioned inelastic hinges, respectively by rotational springs and shear springs. When nonlinear static analyses are performed the strength capacity of the structure is detected when the elastic limit is passed, and the ultimate strength is achieved. In pushover analysis the equivalent linearization technique can be adopted for detecting the capacity curve of the structure. Finally, the EDR is estimated by adopting FEMA 440 and ATC-40 approaches when nonlinear static analyses are performed; the EDR values obtained in such analyses are compared to the one evaluated by nonlinear dynamic analyses (Time History, TH) in which the contribution of single inelastic hinge in terms of hysteretic cycle during the seismic event is considered. Moreover, the EDR values is compared to the transversal displacement optimization to find the best configuration of the roof diaphragm in terms of energy dissipation and EDR as well.

2 NUMERICAL APPROACH

2.1 Structural modelling

Nonlinear dynamic analyses are performed by equivalent finite element model in which mono-dimensional macro-elements represent the parts of the church involved in the nave transversal response [5]. In the one nave configuration church, it is possible to individuate macro-systems able to resist to the transversal earthquake. The macro-systems are the head wall, façade, coupled perimeter walls or triumphal arches (if present). Head wall and façade can be represented by a single vertical equivalent element whereas the coupled perimeter walls or the triumphal arch can be divided in sub-structures, for example in case of single perimeter walls, each sub structure is given by the part of the wall included between lateral openings or the part of wall belonged to a single abutment. The implementation of the equivalent model can be performed by observing the following three steps. In the first step, the sub structures are detected and implemented as single equivalent vertical element. Each sub-structure is divided in sections with fibers discretization; each fiber has nonlinear attributing by concrete trilinear model with zero tensile resistance [10] or the concrete damaged plasticity model ([11], [12]) in which tensile cracking and compressive crushing are the main failure modes [13]; pushover analyses performing on single sub-structure permit to obtain $(M\text{-}\chi)_I$ diagrams describing the behavior of single sub-structure. In the second step, the single sub-structures located on the left and right perimeter walls are implemented and connected themselves by a rigid link located at the top of the elements. The coupled sub-structures represent a transversal resistant system. At the base of the vertical elements, inelastic rotational hinges are located; these hinges are characterized by bi-linear behavior described by yielding and ultimate values already evaluated in $(M\text{-}\chi)_I$. On the system characterized by the coupled sub-structures, pushover analyses are performed again detecting the shear-displacement curves of the transverse resistant system. Consequently, the $(M\text{-}\chi)_{II}$ diagrams of each system are obtained by multiplying and dividing the shear-displacements curves for the shear length (the distance between the section with zero bending moment and the section with maximum bending moment is considered as shear length). Finally, in the third step, the full construction is implemented. The head wall, the façade and the transverse resistant systems are modeled as vertical mono-dimensional equivalent elements by reproducing the in vertical mass distribution of the real elements of the church. Since the façade and the head wall have in-plane

strength and stiffness greater than the longitudinal walls, façade and head walls are fully restrained at the base [14]. At the same time, at the base of the transverse resistant systems, concentrated inelastic rotational hinges are present; these hinges are described by $(M\text{-}\chi)_{II}$ features previously obtained by the pushover analyses of second step. The roof-diaphragm is represented by horizontal mono-dimensional equivalent elements linked to the vertical ones by hinges located at the end of the vertical elements to allow the rocking's trigger and to release the bending moment transferred to the roof. The equivalent elements representing the end parts of the roof are pinned with respect to the head wall and façade. The roof's shear deformability and the nonlinear behavior of the connections are represented shear elastic-plastic hinges. The shear roof springs can be described by trilinear degrading model, Takeda Slip model opportunely modified [15] or by the Clough model in which the unloading stiffness gradually reduces when the deformation increases [16] and [17].

In the equivalent FEM, the earthquake is represented by a set of spectrums compatible accelerograms acting perpendicularly to the nave axis. Once the equivalent model is implemented and the seven-spectrum compatible accelerograms are applied it is possible to evaluate the seismic response for different configurations of the connections.

2.2 Nave transversal response simulation

The implementation of the finite element model described in the previous Section 2.1. permits to simulate the nave transversal response of the church in different configuration of the CLT diaphragm. In fact, CLT panels and connections represent a deformable diaphragm able to permit the rocking trigger of the perimeter walls but also able to limit the lateral displacements and the seismic loads on the rigid head walls when the stiffness of the inelastic shear hinges is opportunely calibrated, working as a roof's damper [18]. The nave transversal response of one nave historical church can be described by a flag-shaped diagram: the response of the seismic resistant elements (see Section 2.1) is represented by bi-linear free rocking curve [5,19] whereas presence of the dissipative hysteretic roof-diaphragm due to the nonlinear behavior of the connections is represented by elastic-plastic curve [20]. The bi-linear behavior of the free rocking can be described by the yielding and ultimate force (respectively $F_{frame,y}$ and $F_{frame,u}$) related to the yielding and the ultimate displacements of the generic resistant seismic frame (respectively $\delta_{frame,y}$ and $\delta_{frame,u}$). These values come out from the pushover analyses of the second step already described in Section 2.1. The stiffness of the frame k_{frame} is consequently given by the ratio between $F_{frame,y}$ and $\delta_{frame,y}$.

The dissipative behavior of the roof can be described by the yielding and the ultimate force (respectively $F_{roof,y}$ and $F_{roof,u}$) related to the yielding and the ultimate displacements of the roof (respectively $\delta_{roof,y}$ and $\delta_{roof,u}$). These values can be determined from experimental tests on the connectors chosen for the connections [21]. The stiffness of the roof k_{roof} is given by the ratio between $F_{roof,y}$ and $\delta_{roof,y}$.

Therefore, by varying the features of the roof diaphragm connections, the roof's stiffness changes and consequently the flag shaped diagram modifies as well. In order to describe the modification of the flag shaped diagram, the hysteretic variables β is introduced [19]; β represents an index of the energy dissipated by the roof (when β increases, the damping effect increases too), consequently it also represents the dissipative capacity of the roof with respect to the features of the masonry walls. The β optimal value could be included in the range $\beta = 0 \div 1.5$ because for higher values the self-centering rocking behavior is partially inhibited having a flag-shaped diagram with significant residual displacements; β is given by the following Equation 1:

$$\beta = 2\frac{F_{roof,y}}{F_{frame,y}} \tag{1}$$

Once β is defined, the yielding force and the stiffness of the roof can be expressed in terms of β, respectively Equation 2 and Equation 3:

$$F_{roof,y} = \frac{\left(F_{frame,y} \cdot \beta\right)}{2} \tag{2}$$

$$k_{roof,y} = k_{frame,y} \cdot \frac{\beta \cdot \delta_{frame,y}}{2 \cdot \delta_{roof,y}} \tag{3}$$

Initially the stiffness of the roof k_{roof} depends on the geometrical and material properties of CLT panels with connections; it is evaluated based on preliminary seismic actions estimation as reported in [18]. The initial k_{roof} is used in the dynamic nonlinear analyses but the optimum roof stiffness ($k_{roof\text{-}opt}$) is detected at the end of the analyses in in correspondence to optimal β value (β_{opt}) able to limit the lateral displacement below the design value (δ_{design})m usually fixed as minor than 0.5% of the perimeter walls' height [18]. The $k_{roof\text{-}opt}$ value can be also expressed by Equation 4 where Δ is the ratio between the yielding displacements of the roof and the frame as it is indicated in Equation 5. It is worth nothing the preliminary approach focused on the limitation of the lateral displacement is crucial for avoiding possible out-of-plane collapse mechanisms [22], also because the stiffness of the roof-diaphragm (introduced in the model by means of the in-plane shear inelastic hinges) affects the maximum lateral displacement. The different configurations of the connections are simulated in the finite element model by varying β.

$$k_{roof-opt} = \frac{\beta_{opt} \cdot k_{frame}}{2 \cdot \Delta} \tag{4}$$

$$\Delta = \frac{\delta_{roof,y}}{\delta_{frame,y}} \tag{5}$$

3 EVALUATION OF THE EFFECTIVE DAMPING RATIO

3.1 Hysteretic models

The Effective Damping Ratio EDR is estimated by adopting FEMA 440 ([1]) and ATC-40 ([2]) approaches in case of nonlinear static analyses and by performing nonlinear dynamic analyses (Time History, TH). In FEMA 440, ATC-40 and TH approaches, the basic hysteretic models to adopt in the EDR estimation must be preliminary defined by assigning the suitable model to the inelastic hinges of the roof-diaphragm in the FEM. Generally, FEMA 440 and ATC-40 individuate four models of Figure 4: Elastic Perfectly Plastic (EPP), Stiffness Degrading (SD) corresponding to a modified Clough [16] in which the lateral stiffness decreases as the level of lateral displacements increases, Strength and Stiffness Degrading (SSD) in which the lateral strength and lateral stiffness decrease when subjected to cyclic reversals. By observing the cycles of connections in shear experimental tests (typically, nails or screws for wood) reproducing the pane-to-panel connections [6] (the more stressed ones in the nave transversal response), the cyclic behavior can be collocated in the halfway between SD and SSD.

Consequently, the inelastic shear hinges of the roof can be described by Clough for SD (characterized by stiffness degradation) and Takeda Slip[23] for SSD model (characterized by strength and stiffness degradation).

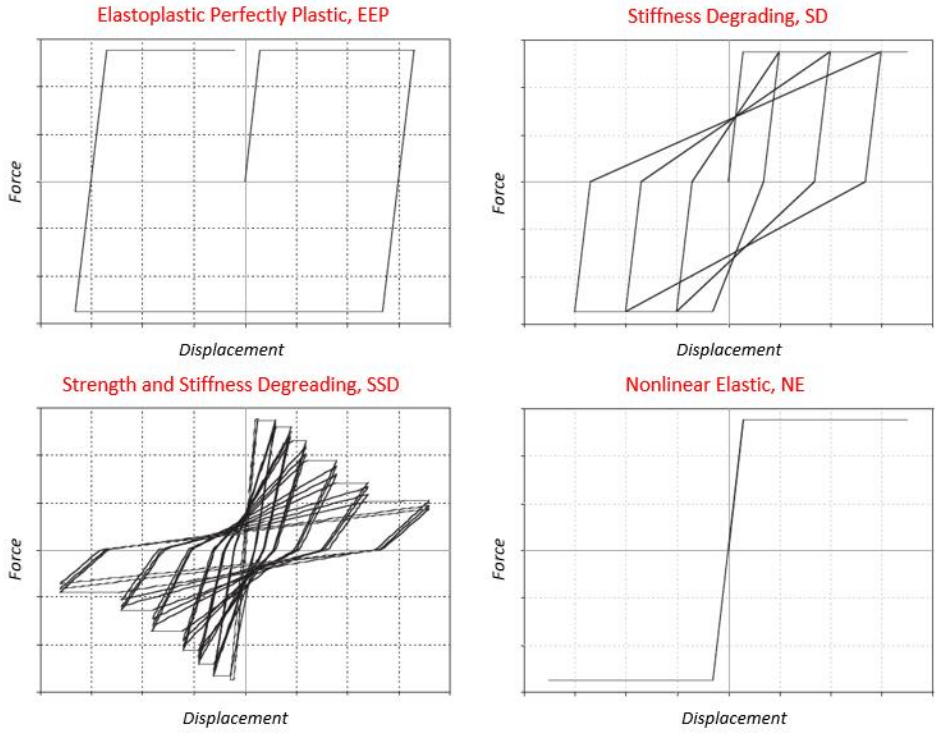

Figure 1 – Hysteretic models

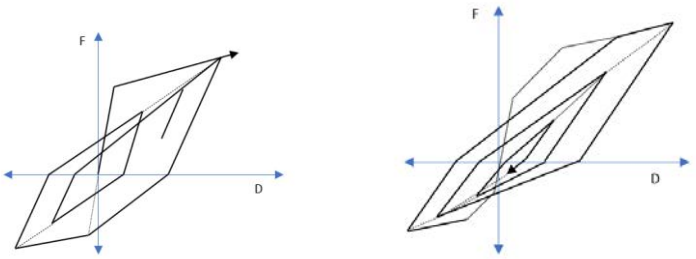

Figure 2 – Clough for SD model on the left and Takeda slip for SSD model on the right.

3.2 FEMA 440

In FEMA 440, EDR is estimated by equivalent linear method in which the period of the structure is evaluated from the initial vibrational period of the nonlinear system and the maximum ductility ratio μ. EDR depends on μ, the post-yield stiffness ratio α and a sort of adjustment factor k considering changes in hysteretic behavior, [1]. FEMA 440 indicates three kinds of behavior called Type A, Type B and Type C, respectively corresponding to the previous shown models EEP (without degrading), SD (stiffness degrading) and SSD (strength and stiffness degrading). In this paper, as suggested by ATC-40, the analyses consider that the initial elastic viscous damping ratio of the construction is 0.05 (5%). Consequently, EDR is estimated by Equation 6 in which the terms to the right of k are the equivalent hysteretic viscous damping for an idealized bilinear system (also called β_0 in ATC-40). When the Clough model

is adopted k = 0.67 considering the stiffness degradation, whereas Takeda slip is used k = 0.33 considering the stiffness and strength degradation. It is worth nothing that EDR corresponds to the Effective Viscous Damping called β_{eq} in ATC-40.

$$EDR = 0.05 + k \cdot (2/\pi) \cdot \{[(\mu-1) \cdot (1-\alpha)] / [\mu \cdot (1+ \alpha \cdot \mu - \alpha)]\} \quad (6)$$

3.3 ATC-40

EDR estimation by ATC-40 is based on the Capacity Spectrum Method of Equivalent Linearization in which the maximum inelastic deformation of a nonlinear system is approximated from the maximum deformation of a linear elastic system having a period and damping ratio larger than the initial values of those of the nonlinear system. The Capacity Spectrum Method gives a force-deformation relationship for the structure. By the Capacity -Spectrum Method of equivalent linearization, EDR is graphically given by Figure 6 and Equation 7 in which: E_d is the energy dissipated by damping (corresponding to the area enclosed by hysteresis loop), E_{S0} is the maximum strain energy (graphically given by the area enclosed in the triangle defined by spectral displacement d_{pi} and the spectral acceleration a_{pi} of the performance point). The equivalent period, T_{eq}, is assumed to be the secant period at which the seismic ground motion demand, reduced for the equivalent damping, intersects the capacity curve.

$$EDR = (1/4\pi) \cdot (E_d / E_{S0}) \quad (7)$$

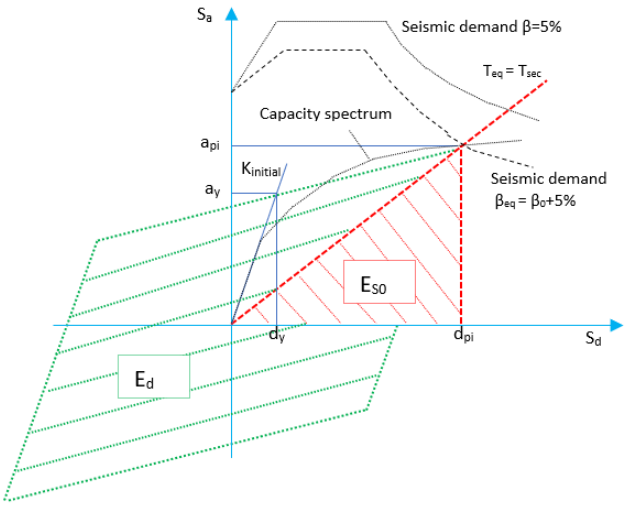

Figure 3 – EDR estimation by FEMA 440 and ATC-40

3.4 TH method

By TH method, EDR can be estimated by considering the cycles of the inelastic hinges of the walls and roof during the seismic events. Each inelastic hinge able to dissipate energy shows different closed cycles during the seismic event. Knowing the previous control nodes of FEMA 440 and ATC-40, when the generic control node is known, its lateral displacement's time history can be plotted, and the following instants (points 0÷4 of Figure 4) can be detected to determinate the enclosed cycle of the inelastic hinges. The first instant corresponds to the one in which the control node achieves for the first time during the seismic events the control displacement value already evaluated in FEMA or in ATC (point 1 in Fig-

ure 4). The second time instant is located before point 1 on the x-time axis; it represents the origin of the cycle, and it corresponds to the previous instant in which the displacement's time history meets the time axis (point 0 in Figure 4).

The following instants correspond to the maximum transversal displacements in both positive and opposite verse (points 2 and 3 in Figure 4). The last time instant corresponds to the end point of the cycle occurring when the displacement's time history meets again the time axis (point 4 in Figure 4). Consequently, the time instants of points 0÷4 are used to define the enclosed sub-cycle to extract from all the cycles representing the behaviors of each inelastic hinge (both for walls and roof). Each enclosed sub-cycle is included in the time instants already found in 1÷4 points (Figure 4).

For each inelastic hinge present on the roof, the inner area of the related enclosed sub-cycle represents the damping energy dissipated by the inelastic hinge (E_D). When the sub-cycle is drawn the maximum transversal displacements can be detected either along the seismic direction and in the opposite one. In correspondence of the maximum displacement value, the maximum strain energy (E_{S0}) of the enclosed sub-cycle can be calculated. The value of E_{S0} is graphically calculated as the area enclosed in the triangle given by the origin point, the point corresponding to the maximum displacement and its vertical projection on the x-time axis. When the inelastic hinges do not give a contribute in terms of damping energy, enclosed sub-cycles do not exist; however, in these cases, the inelastic hinges are considered for their contribution in terms of strain energy (graphically evaluated as previously mentioned).

Therefore, by considering all the inelastic hinges of the walls and roof, the EDR of the entire structure can be estimated by Equation 6 where i represents the number of the inelastic hinges of the roof and the walls, E_D and E_{S0} respectively are the damping energy and the maximum strain energy of the i-th inelastic hinge evaluated in the time range extracted from the transverse displacement's time history of the control node defined by FEMA 440 or ATC-40. The graphically procedure illustrated in Figure 4 is performed for all the inelastic hinge under the seven-spectrum compatible accelerogram. The value to consider for the EDR estimation is the average one. Thus, in Equation 6 the average values of E_D and E_{S0} are considered.

$$\boldsymbol{EDR} = \frac{1}{4\pi}\frac{\sum_{i=1}^{n}(\boldsymbol{E_D})_i}{\sum_{i=1}^{n}(\boldsymbol{E_{S0}})_i} \tag{6}$$

The strategy here considered to evaluate the most suitable solution for the roof diaphragm by the TH approach is based on the hysteretic variable β introduced in Section 2.2. By changing β values in the range $0< \beta <1.5$ it is possible to simulate by FEM different roof diaphragm configuration to evaluate the seismic response under the seven spectrum compatible aerograms in terms of transversal displacements. By this way the optimal β_{opt} value able to minimize the displacements without extremely increase the forces transmitted on the façade can be found. In parallel, by varying β, the response of the one nave church can be studied in terms of transversal displacement of the control node previously detected in FEMA 440 and ATC-40.

As it is above mentioned, once the transversal displacements' time histories of the control nodes are plotted for several β values, for each inelastic hinges in the FEM the cyclic behaviors are plotted as well and the sub-cycles to consider for EDR evaluation can be drawn. Finally, EDR can be analyzed in relation to the hysteretic variable β, and its trend can be compared to the one of the transversal displacements of the roof's central node (corresponding to the roof's part with the maximum deformation in the nave transversal response).

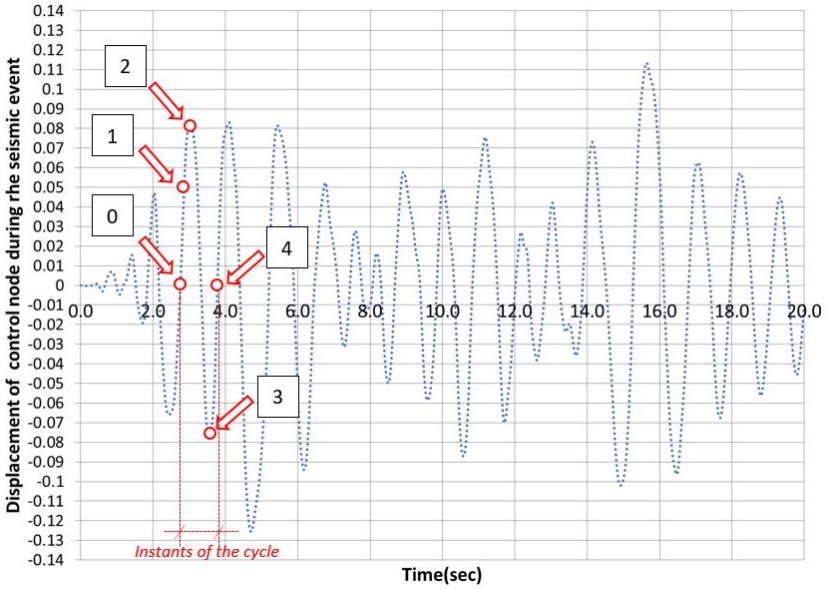

a)

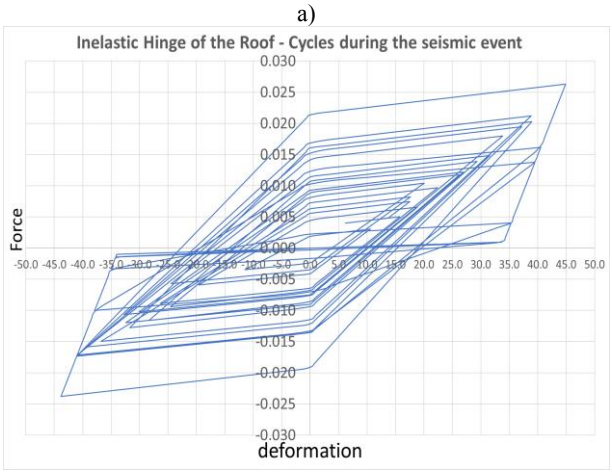

b)

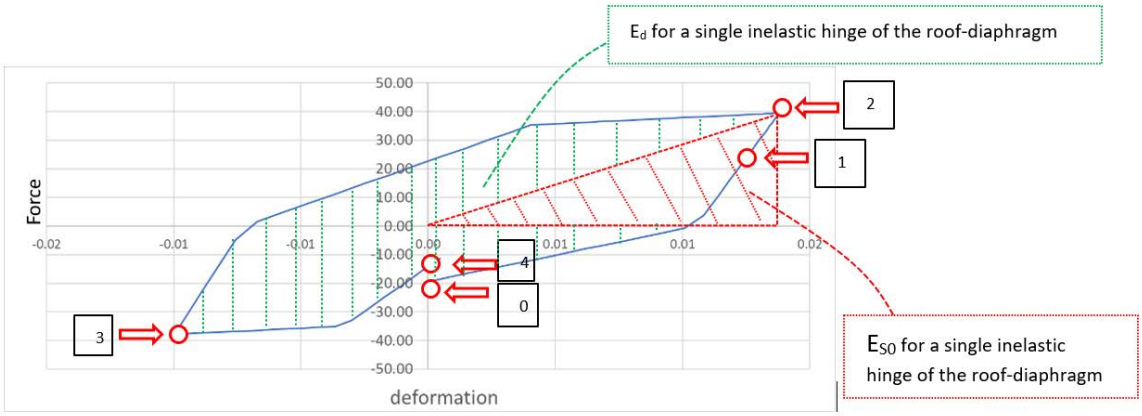

c)

Figure 4 – Definition of cycles for the inelastic hinges of the FEM: a) transversal displacement of the control node evaluated by FEMA or ATC during the seismic event – individuation of the points representing the cycle to consider; b) cycle of a generic inelastic hinge of the roof able to dissipate energy during the seismic event (in figure Clough model is adopted) – c) extrapolation of the single cycle to consider for evaluating the contribute of the roof's generic inelastic hinge in terms of energy dissipating by damping E_d and maximum strain energy E_0.

4 CASE STUDY

The EDR evaluation is here performed for a single nave configuration church with masonry walls and wooden roof. The church has a 33m x 12m rectangular plan 0.90 m thickness head wall and façade, 0.60m thickness perimeter walls. The roof is characterized by hardwood trusses (a general branch is represented in Figure 8), and three openings are present in the perimeter walls (Figure 8). The masonry is characterized by Young modulus E = 1200 MPa and weight density ρ = 18 kN/m^3. The equivalent FEM is represented by monodimensional equivalent elements representing the walls and the roof. The rotational inelastic hinges are located at the base of the vertical elements whereas the in-plane shear inelastic hinges are in the middle of the equivalent horizontal elements (Figure 8). Since the different distances among the vertical equivalent elements, there are two different values for the inelastic hinges located close the head wall and façade with respect to the others located in the central part of the roof. Starting from the design target behavior in which the energy dissipation in the steel connections of the roof occurs when the inelastic hinges of the walls achieve the yielding point, the yielding and ultimate values attributing to the inelastic hinges' properties are shown in Table 1. The properties vary by hysteretic variable β while the properties of the inelastic hinges characterizing the masonry elements are evaluated as already described in Section 2.1. Table 1 resumes the inelastic hinges properties either for the walls (subscript frame) and the roof (symbol P1-D1 and P2-D2).

In Table 1, P1 and P2 respectively indicate the yielding and the ultimate force of the roof's inelastic hinges; D1 and D2 respectively are dimensionless values given by the ratio between the yielding or the ultimate deformations and the length of the church (symbol l in Table 1). P1-D1 and P2-D2 are used in Clough in case of SD model is adopted. When the Takeda slip is attributed to the inelastic hinges, three points P1-D1, P2-D2 and P3-D3 must be defined.

In [23], since the Takeda is normally adopted for reinforced concrete structure, it is possible to assume P2-D2 as the yielding points already found for the Clough, P3-D3 as the ultimate points already evaluated for the Clough, with P1-D1values (usually the cracking point) very close to the yielding ones. For the sake of brevity, the Takeda values are not present in Table 1.

In the case study the CLT panels have 6cm thickness with three 2 cm thickness layers. In the FEM the equivalent horizontal elements take in account the CLT panels' total thickness while the dead load due to the wooden beams is considered by the element beam loads uniformly applied. Also, the in-elevation part of the façade is applied as nodal load on the top of the equivalent vertical element representing the façade.

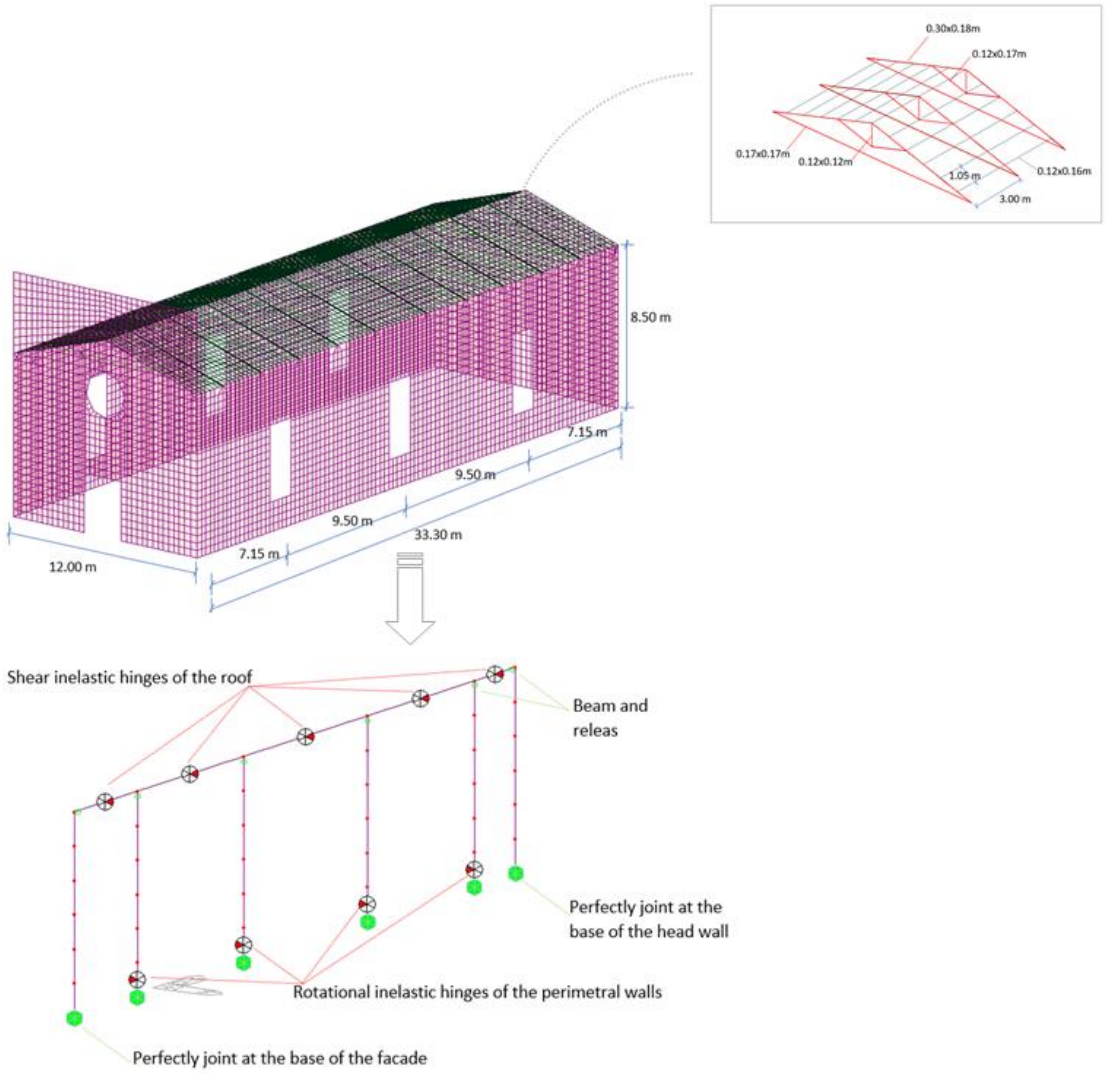

Figure 5: case study and FEM.

Parts of the roof close to the head wall and facade							
β	P_1 [kN]=$F_{roof,y}$	P_2 [kN]=$F_{roof,u}$	$D_1=(P_1/K_{roof,y})/l$	D_2	$M_{frame,y}=M_{frame,u}$ [kNm]	$R_{frame,y}$ [rad]	$R_{frame,u}$ [rad]
0.30	9.69	12.11	0.00062	0.01257	555.422	0.00086	0.00258
0.60	19.38	24.22	0.00062	0.01257	555.422	0.00086	0.00258
0.90	29.06	36.33	0.00062	0.01257	555.422	0.00086	0.00258
1.20	38.75	48.44	0.00062	0.01257	555.422	0.00086	0.00258
1.50	48.44	60.55	0.00062	0.01257	555.422	0.00086	0.00258
1.80	58.13	72.66	0.00062	0.01257	555.422	0.00086	0.00258
2.10	67.81	84.77	0.00062	0.01257	555.422	0.00086	0.00258
Central parts of the roof							
β	P_1 [kN]=$F_{roof,y}$	P_2 [kN]=$F_{roof,u}$	$D_1=(P_1/K_{roof,y})/l$	D_2	$M_{frame,y}=M_{frame,u}$ [kNm]	$R_{frame,y}$ [rad]	$R_{frame,u}$ [rad]
0.3	189.72	237.15	0.008619834	0.17239	10877.185	0.01182	0.03548
0.6	379.44	474.30	0.008619834	0.17239	10877.185	0.01182	0.03548
0.9	569.16	711.44	0.008619834	0.17239	10877.185	0.01182	0.03548
1.2	758.87	948.59	0.008619834	0.17239	10877.185	0.01182	0.03548
1.5	948.59	1185.74	0.008619834	0.17239	10877.185	0.01182	0.03548
1.8	1138.31	1422.89	0.008619834	0.17239	10877.185	0.01182	0.03548
2.10	1328.03	1660.04	0.008619834	0.17239	10877.185	0.01182	0.03548

Table 1: properties of the inelastic hinges

5 RESULTS

The transversal displacements are investigated in relation to the hysteretic variable β by fixing the target displacement referring to the 5% of the total height of the walls (in the case study the target displacement is 0.043m). It is considered β varies in the range 0÷2.1 to deep the seismic response also for values higher than the limit value 1.5 corresponding to an over-stiffness condition of the roof. Figure 6 shows the optimal value of the hysteretic variable is around β_{opt} =1.35; beyond β_{opt} the transversal displacement values not significantly decrease as it occurs in the previous branch of the diagram. Once the transversal displacements are investigated, FEMA 440 and ATC-40 approaches are used to evaluate EDR by pushover analyses (PO) for different β values and by considering SD and SSD models for the inelastic hinges' properties. PO analyses are performed therefore in FEMA 440 and ATC-40 the control nodes are detected and their displacements are evaluated as well (Table 2).

The node numbers indicated as 57 and 64 of Table 2 corresponds to the nodes determining the central beam element of the roof, present in the equivalent FEM, already shown in Figure 8. In the present case study, PO performed by FEMA 440 and ATC-40, EDR is estimated by adopting Procedures A. The EDR values detected by FEMA 440 and ATC-40 are plotted in Figure 7 and Figure 8 in relation to the hysteretic variable and in comparison to the values obtained by TH approach (which separately considers the control nodes and their displacements detected in FEMA440 and the ones of ATC-40).

From Figure 7 and Figure 8 the EDR evaluated by PO of FEMA 440 and ATC-40 are generally higher than the values evaluated by TH approach. The importance of the hysteretic model for the inelastic hinges of the roof are appreciable. In fact, the EDR values estimated

by SD model are higher than the ones of SSD model, as a consequence in SD model there is a higher percentage of the dissipated energy during the seismic event by the roof-diaphragm. EDR values of SD model are higher than the SSD ones. The difference between SD and SSD models is more evident for ATC-40 approach.

For all of the estimations, the range $0.3< \beta< 1.2$ shows a quasi-linear trend whereas the $1.2< \beta<1.5$ range shows a spike of EDR values. Once passed $\beta<1.5$ the energy dissipation due to the roof diaphragm is not significative, consequently the range $1.5<\beta<2.1$ is almost constant and even in ATC-40 and TH referring to ATC-40 the EDR decreases in this branch.

EDR's values evaluated by PO are overestimated especially in SD model for ATC-40.

Generally, the EDR trends detected by TH approaches (by considering either the FEMA 440 or ATC-40 control nodes) are similar to the one of the transversal displacements.

Finally, for the case study here presented, in the correspondence of the hysteretic variable's optimal value, the EDR values are shown in Table 3.

β	Approach	Control node	Control node - displacement [m]
0.3	PO-FEMA / PO-ATC	64/64	0.0382 / 0.0552
0.6	PO-FEMA / PO-ATC	64/64	0.0289 /0.0510
0.9	PO-FEMA / PO-ATC	64/64	0.0297 /0.0442
1.2	PO-FEMA / PO-ATC	64/64	0.0272 /0.0450
1.5	PO-FEMA / PO-ATC	57/57	0.0374 /0.0548
1.8	PO-FEMA / PO-ATC	57/57	0.0357 /0.0505
2.1	PO-FEMA / PO-ATC	64/64	0.0212 /0.039

Table 2: identification of the control nodes and their displacements by FEMA 440 (FEMA) and ATC-40 (ATC).

Approach	Model	EDR [%] ($\equiv \beta_{eq}$ FEMA 440, β_{eff} in ATC-40)
FEMA 440	SD	≃16.8
ATC-40	SD	≃25.0
TH refers to FEMA 440	SD	≃15.2
TH refers to ATC-40	SD	≃14.8
FEMA 440	SSD	≃ 16.0
ATC-40	SSD	≃16.3
TH refers to FEMA 440	SSD	≃12.5
TH refers to ATC-40	SSD	≃12.1

Table 3: EDR' values for the case study (considering inelastic properties of the walls and roof) for the optimal value of the hysteretic variable $\beta_{opt} = 1.35$

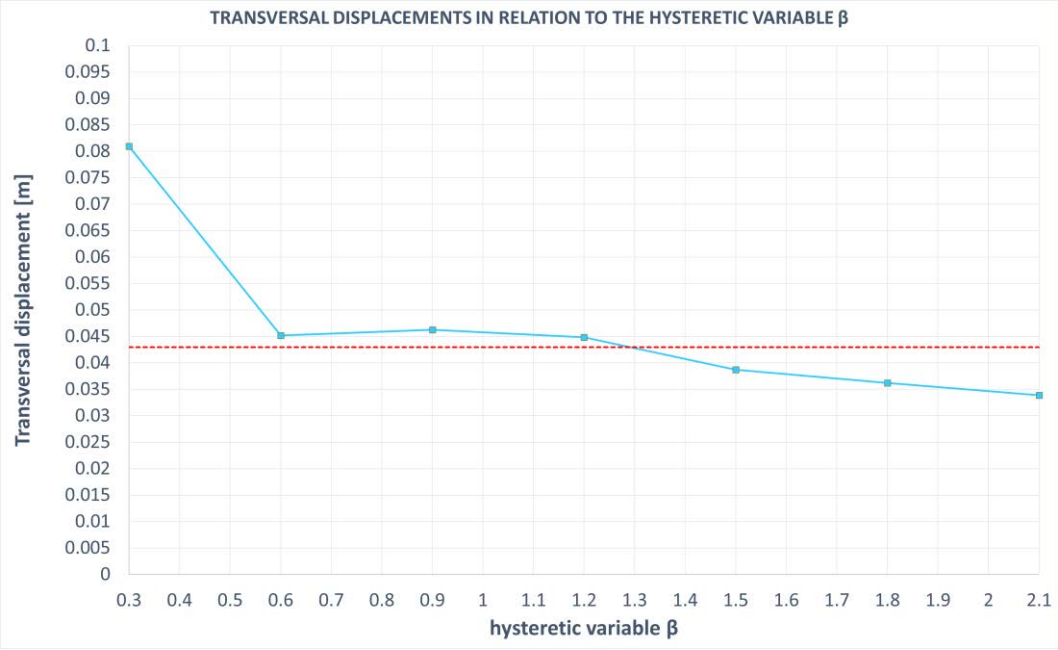

Figure 6: average values of the transversal displacements of the roof's central part under seven spectrum-compatible accelerograms.

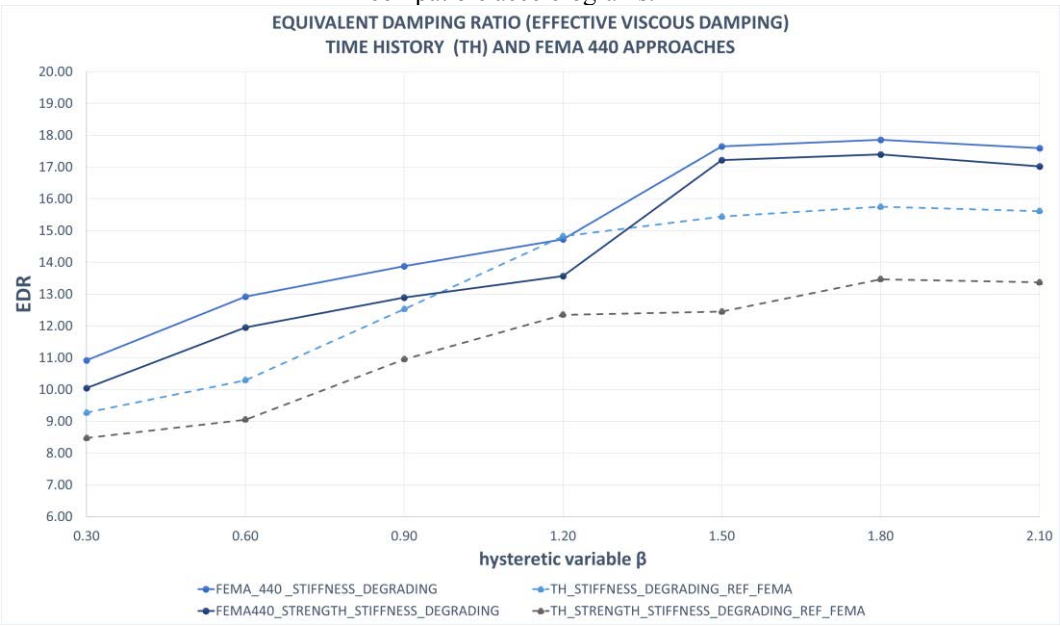

Figure 7: EDR evaluation by TH and FEMA 440 in relation to the hysteretic variable β in case of stiffness degrading SD and strength and stiffness degrading SSD hypotheses.

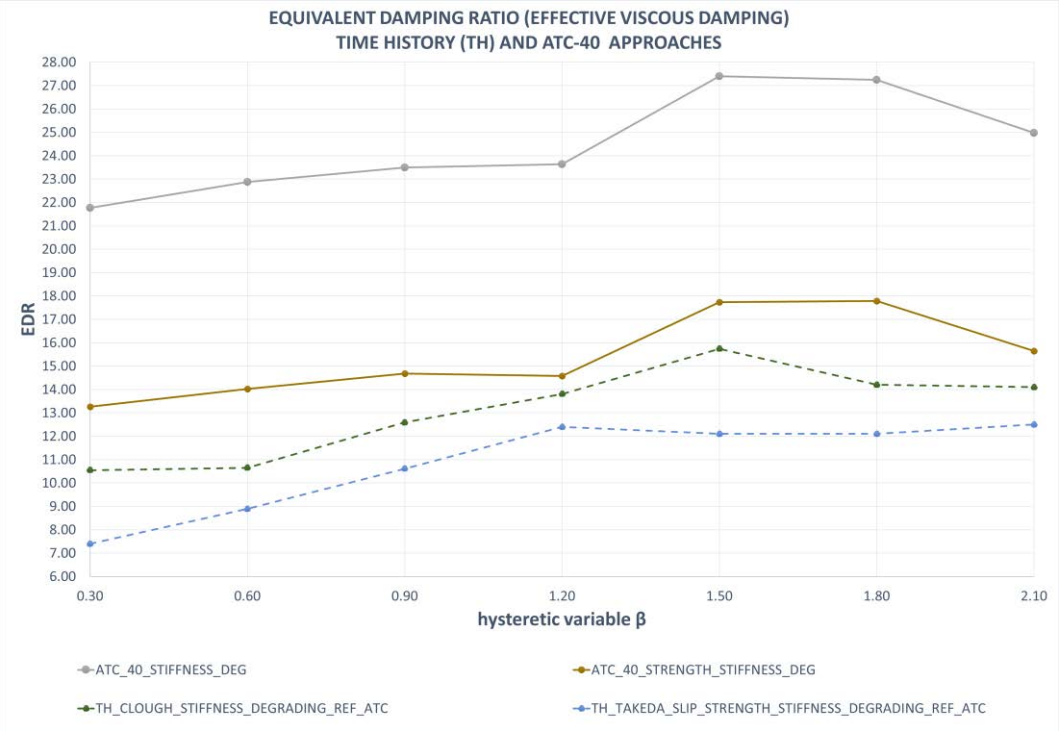

Figure 8: EDR evaluation by TH and ATC-40 in relation to the hysteretic variable β in case of stiffness degrading SD and strength and stiffness degrading SSD hypotheses.

6 CONCLUSIONS

In this paper the evaluation of the Equivalent Damping Ratio (EDR), also called equivalent damping in FEMA 440 or effective damping in ATC-40, is performed in the nave transversal response under a seismic event for a one nave configuration church (with masonry walls and CLT roof structure). The seismic response in studied adopting equivalent finite element model (Section 2.1) in terms of hysteretic variable β (Section 2.2) and by considering different models for the inelastic hinges of the roof (in particular Stiffness Degrading SD and Strength and Stiffness Degrading SSD, Section 3.1). EDR is evaluated by nonlinear static analyses (pushover analyses PO) by FEMA 440 and ATC-40, (Section 3.2 and Section 3.3) and nonlinear dynamic analyses by a Time Histories (TH) approach described in Section 3.4.

TH approach considers the control nodes and their displacements previously identified by FEMA 440 and ATC-40. Once the optimal values of the hysteretic variable β_{opt} is detected, the target transversal displacement (5% of the perimeter walls' height), in correspondence of β_{opt}, the corresponding EDR is evaluated as well, by FEMA 440, ATC-40 and TH approaches. The results show:

- The EDR's variation in relation to the hysteretic variable β is very similar to the transversal displacements' one by performing nonlinear dynamic analysis.
- TH approach gives EDR values minor than the ones evaluated by FEMA 440 and ATC-40.
- The effects of SD and SSD models are significant in terms of dissipated energy during the seismic event.
- ATC-40 overestimates EDR values, especially if SD model is adopted.
- Generally, the TH approach gives EDR values minor the ones of FEMA 440 and ATC-40.
- The optimal β_{opt} value detected in the transversal displacements diagram is also valid in the EDR estimation.

- Over $\beta = 1.5$ the dissipative effects of the roof-diaphragm decades testifying the important role of the dissipative roof-diaphragm in comparison to an over-stiffness configuration.

REFERENCES

[1] FEMA. No Title. FEMA 440 Improv Nonlinear Static Seism Anal Proced 2005.

[2] ATC 40. SEISMIC EVALUATION AND RETROFIT OF CONCRETE BUILDINGS ATC -40. ATC 40 Rep SSC 96-01 n.d.;1.

[3] Milani G. Lesson learned after the Emilia-Romagna, Italy, 20-29 May 2012 earthquakes: A limit analysis insight on three masonry churches. Eng Fail Anal 2013. https://doi.org/10.1016/j.engfailanal.2013.01.001.

[4] Liberatore D, Doglioni C, AlShawa O, Atzori S, Sorrentino L. Effects of coseismic ground vertical motion on masonry constructions damage during the 2016 Amatrice-Norcia (Central Italy) earthquakes. Soil Dyn Earthq Eng 2019. https://doi.org/10.1016/j.soildyn.2019.02.015.

[5] Longarini, Nicola,CRESPI , PIETRO, ZUCCA M. The influence of the geometrical features on the seismic response of historical churches reinforced by different cross lam roof-solutions. Bull Earthq Eng 2022;20:6813–6852.

[6] Angelo Aloisio; Rocco Alaggio; and Massimo Fragiacomo. Equivalent Viscous Damping of Cross-Laminated Timber Structural Archetypes. J Struct Eng 2021;147(4): 04.

[7] Longarini N, Crespi P, Zucca M. Dissipative cross lam roof structure for seismic restoration of historical churches. REHABEND, 2018.

[8] Longarini N, Crespi P, Scamardo M. Numerical approaches for cross-laminated timber roof structure optimization in seismic retrofitting of a historical masonry church. Bull. Earthq. Eng., 2020. https://doi.org/10.1007/s10518-019-00661-w.

[9] EUROCODE 5 Design of timber structures UNI EN 1995-1-1. 1995.

[10] Midas. Midas GEN FX Program - General structure design system n.d.

[11] Lubliner J, Oliver J, Oller S, Oñate E. A plastic-damage model for concrete. Int J Solids Struct 1989. https://doi.org/10.1016/0020-7683(89)90050-4.

[12] Lee J, Fenves GL. Plastic-Damage Model for Cyclic Loading of Concrete Structures. J Eng Mech 2002. https://doi.org/10.1061/(asce)0733-9399(1998)124:8(892).

[13] Valente M, Milani G. Damage assessment and partial failure mechanisms activation of historical masonry churches under seismic actions: Three case studies in Mantua. Eng Fail Anal 2018. https://doi.org/10.1016/j.engfailanal.2018.06.017.

[14] Preti M, Bolis V, Marini A, Giuriani E. Example of the Benefits of a Dissipative Roof Diaphragm in the Seismic Response of Masonry. Proc 9th Int Conf Struct Anal Hist Constr 2014.

[15] Barbosa MJ, Pauwels P, Ferreira V, Mateus L. Towards increased BIM usage for

existing building interventions. Struct Surv 2016. https://doi.org/10.1108/SS-01-2015-0002.

[16] Genshu T, Yongfeng Z. Seismic force modification factors for modified-Clough hysteretic model. Eng Struct 2007;29:3053–70. https://doi.org/10.1016/j.engstruct.2006.12.007.

[17] Hossain A, Lakshman R, Tannert T. Shear Connections with Self-Tapping Screws for Cross-Laminated Timber Panels, 2015. https://doi.org/10.1061/9780784479117.195.

[18] Giuriani E, Marini A. Wooden roof box structure for the anti-seismic strengthening of historic buildings. Int J Archit Herit 2008. https://doi.org/10.1080/15583050802063733.

[19] Preti M, Loda S, Bolis V, Cominelli S, Marini A, Giuriani E. Dissipative Roof Diaphragm for the Seismic Retrofit of Listed Masonry Churches. J Earthq Eng 2017. https://doi.org/10.1080/13632469.2017.1360223.

[20] Johansen KW. Theory of Timber Connections. IABSE Int Assoc Bridg Struct Eng 1949.

[21] Sandhaas C, van de Kuilen JWG. Strength and stiffness of timber joints with very high strength steel dowels. Eng Struct 2017. https://doi.org/10.1016/j.engstruct.2016.10.046.

[22] Giuriani EP, Marini A, Preti M. Thin-folded Shell for the Renewal of Existing Wooden Roofs. Int J Archit Herit 2016. https://doi.org/10.1080/15583058.2015.1075626.

[23] Takeda T. Reinforced Concrete Response to Simulated Earthquakes 1971.